Naval Research Laboratory
Washington, DC 20375-5320

NRL/MR/6755--98-8171

The Effects of Neutral Gas Release on Vehicle Charging: Experiment and Theory

D.N. WALKER
W.E. AMATUCCI
R.F. FERNSLER
C.L. SIEFRING
M.J. KESKINEN

Charged Particle Physics Branch
Plasma Physics Division

J.H. BOWLES
J.A. ANTONIADES

Remote Sensing Studies and Simulation Branch
Remote Sensing Division

October 30, 1998

REPORT DOCUMENTATION PAGE

Form Approved
OMB No. 0704-0188

1. AGENCY USE ONLY (*Leave Blank*)	2. REPORT DATE	3. REPORT TYPE AND DATES COVERED
	October 30, 1998	Interim

4. TITLE AND SUBTITLE

The Effects of Neutral Gas Release on Vehicle Charging: Experiment and Theory

5. FUNDING NUMBERS

6. AUTHOR(S)

D.N. Walker,* W.E. Amatucci,* J.H. Bowles,** R.F. Fernsler,* C.L. Siefring,* J.A. Antoniades,** and M.J. Keskinen*

7. PERFORMING ORGANIZATION NAME(S) AND ADDRESS(ES)

Naval Research Laboratory
Washington, DC 20375-5320

8. PERFORMING ORGANIZATION REPORT NUMBER

NRL/MR/6755--98-8171

9. SPONSORING/MONITORING AGENCY NAME(S) AND ADDRESS(ES)

Office of Naval Research
800 N. Quincy Street
Arlington, VA 22217-5660

10. SPONSORING/MONITORING AGENCY REPORT NUMBER

11. SUPPLEMENTARY NOTES

*Plasmas Physics Division
**Remote Sensing Division

12a. DISTRIBUTION/AVAILABILITY STATEMENT

Approved for public release; distribution unlimited.

12b. DISTRIBUTION CODE

13. ABSTRACT (*Maximum 200 words*)

This paper describes an experimental and theoretical research effort related to the mitigation of spacecraft charging by Neutral Gas Release (NGR). Laboratory simulations which employ a charged aluminum cylinder containing a neutral gas release valve have verified the effectiveness of NGR as a means of mitigating high voltages under environmental conditions close to the natural space environment. The charging electronics were developed under the Space Experiment Aboard Rockets (SPEAR) program. The experiments were conducted in the large volume Space Physics Simulation Chamber (SPSC) at the Naval Research Laboratory. This Laboratory environment is similar to that encountered by LEO spacecraft, e.g., the Space Station, Shuttle, and high inclination satellites. The basis of the theoretical treatment is a simple Townsend discharge. In addition the nozzle release of neutral gas is modeled and a simple linear spatial dependence of the applied potential is assumed. This basic model produces quite good results when compared to the experiment.

14. SUBJECT TERMS

Vehicle Charging
Active experiments
Neutral gas release

15. NUMBER OF PAGES

30

16. PRICE CODE

17. SECURITY CLASSIFICATION OF REPORT	18. SECURITY CLASSIFICATION OF THIS PAGE	19. SECURITY CLASSIFICATION OF ABSTRACT	20. LIMITATION OF ABSTRACT
UNCLASSIFIED	UNCLASSIFIED	UNCLASSIFIED	UL

NSN 7540-01-280-5500

Standard Form 298 (Rev. 2-89)
Prescribed by ANSI Std 239-18
298-102

TABLE OF CONTENTS

THE EFFECTS OF NEUTRAL GAS RELEASE ON VEHICLE CHARGING: EXPERIMENT AND THEORY

I. Introduction

As is well-known, spacecraft in LEO can acquire large negative potentials relative to the local plasma, and these potentials can damage sensitive spacecraft electronics even in the absence of active experimentation as, for example, in the case of solar arrays [*McPherson et al.,1976; Hastings et al., 1992].* Such large negative voltages can be acquired by movement through natural environments such as the auroral regions *[Gussenhoven et al., 1985; Mullen et al., 1986],* or because of active space experiments which emit a charged particle beam when insufficient neutralizing return current is collected *[Borovsky, 1988].* For example, at negative charging levels the low mobility of positive ions impedes their ability to act as neutralizing return current. Another source of payload charging is ion beam emission *[Kaufmann et al., 1989; Roth et al., 1983],* but typically the currents are small and charging has not been observed above a few hundred volts *[Olsen et al., 1990].* However, electron beam sources employed in many space experiments are capable of relatively large currents and they can also cause high-voltage charging; both positive and negative charging is predicted to occur because of ringing *[Borovsky, 1988; Winglee, 1991].* Also, satellites in eclipse in the auroral region, for example, and geosynchronous spacecraft can often reach high negative voltage levels. These voltages can reach hundreds of volts and have been observed as high as several kilovolts. In addition, planned charging and discharging events typically produce a rapid change in the payload potential with a slow decay to equilibrium so that large potentials can occur, for example, on the LEO spacecraft solar arrays mentioned above *[Hastings et al., 1992].* Conventionally, most solar array systems for U.S. space vehicles have a bias of 28 Volts. Future solar arrays, however, are being designed for much higher voltages to meet higher power demands at low currents. The space station, for example, has 160 Volt arrays. Resulting electrical discharges in solar arrays have led to performance losses in several recent satellite launches.

Because of the above considerations and the active nature of desired experimentation, much of the focus of the Space Power Experiments Aboard Rockets (SPEAR) III program was the study of a variety of spacecraft grounding techniques. This was part of the overall objective of investigating the interaction of high voltage power systems in the low earth orbit (LEO) environment. The SPEAR program was begun by the Ballistic Missile Defense Organization (BMDO) in the late 1980's and continued with the successful launches of two sounding rockets, in addition to a series of ground tests in large laboratory environments *[Berg et al., 1995; Gilchrist et al., 1993; Greaves et al., 1990; Alport et al., 1990*]. Several of the results from these tests showed promising possibilities for mitigation of the charging through neutral gas release *[Berg et al., 1995].* An attractive feature of this method lies in the fact that most spacecraft have relatively large amounts of neutral gas storage, often for the purpose of attitude control adjustments. Therefore, if this reservoir can be used in mitigation techniques it might provide a means of ameliorating the charging without the incorporation of specially designed systems (such as plasma thrusters). Recent results *[Mandel et al., 1998; Machuzak et al., 1996; Berg et al., 1995; Gilchrist; 1993; 1990]* suggest that this approach may hold promise in typical operational scenarios, both in rocket flights and Space Shuttle configurations.

Manuscript approved July 15, 1998.

This paper describes laboratory experiments designed to investigate the effects of Neutral Gas Release (NGR) on space vehicle charging. The effort is an outgrowth of the SPEAR program. The experimentation includes use of a simulated "payload" cylinder which is situated in a large vacuum chamber at the Naval Research Laboratory (NRL) and which incorporates a neutral gas release valve. The cylinder and valve are charged to kilovolt levels (usually negative) with respect to the chamber walls, both in vacuum and in plasma environments, and the neutral gas is released, resulting in discharge, or breakdown, to the local plasma. The charging electronics package, which was built at NRL, was used in the SPEAR laboratory testing and was afterward refitted for use in the Space Physics Simulation Chamber (SPSC). The experiment consists of varying the mass of the release gas, composition, flow rate and mach number of the releases and determining the effects on final voltage and voltage discharge initiation levels.

The theoretical treatment of the discharge is treated through an analysis which employs the Townsend discharge criterion. The fundamental assumption in this model is that when a negatively charged object in neutral gas discharges (or when the discharge takes place from the cathode to the anode) the number of electrons grows exponentially in an avalanche fashion along the discharge path. The model then is highly neutral gas dependent through the Townsend ionization coefficient which is defined as the number of ionization events occurring per unit length in the electric field direction. In addition, the nozzle shape and design have a fundamental effect on the neutral gas distribution and therefore on the discharge characteristics. We treat these areas in a simple model which, through flux conservation and the assumption of isentropic expansion upon release, appears to successfully model the physics of the release and its relation to the subsequent discharge.

II. Experimental Description

The experimentation was performed in the Naval Research Laboratory's Space Physics Simulation Chamber (SPSC) using an existing diagnostic complement developed for this and other programs. One particular advantage of this experimental environment is the large size of the facility (1.8 m x 5 m vacuum chamber) in addition to the ability to produce plasma conditions approaching those of the natural ionosphere. Size is important for eliminating wall effects, and parameters approaching ionospheric LEO values are important for relevance to space concerns.

ChamberEnvironment

The SPSC is a 1.8-m diameter by 5-m long cylindrical vacuum chamber shown in Figures 1 and 2 which can be evacuated to a background pressure near 10^{-6} torr.

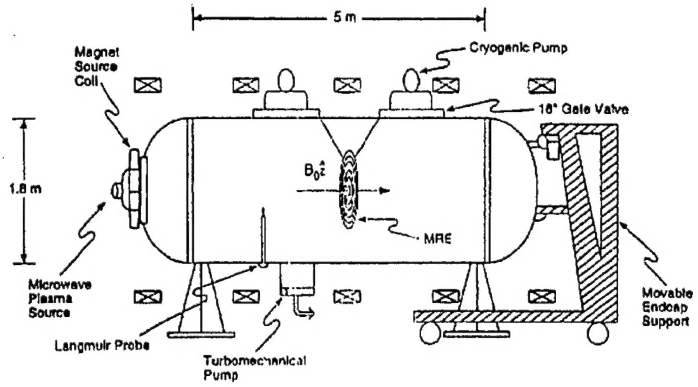

Figure 1

Coils arranged in an approximate Helmholtz configuration provide an axial magnetic field variable up to 50 G. There is the capability to pulse the field to kilogauss levels. Multiple ports and an internal 3D positioning system are available for diagnostic access. The chamber is equipped with two microwave plasma sources *[Walker et al., 1994; Bowles et al., 1996]* designed with different output areas for density variation and differing experimental requirements. The wide area microwave plasma source is shown in Figure 3. In addition there are filament sources which can provide densities as high as 10^{12} cm^{-3}. A variety of experiments simulating space plasma phenomena have been performed in the chamber *[Walker et al., 1995, 1997; Amatucci et al., 1996, 1998a,b]*

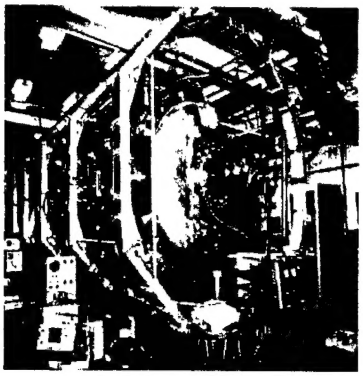

Figure 2

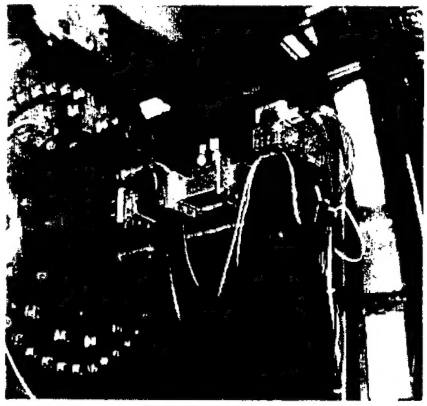

Figure 3

Table I outlines the basic plasma parameters for a 50-cm diameter argon plasma column. The parameters are close to the LEO environment so that scaling concerns in this chamber are a minimum. While the ion-electron temperature ratio is lower than in the ionosphere, the base ion temperature does correspond well to that in the ionosphere. Also, changes in operating conditions for the microwave plasma source (such as operation under higher background pressures) are expected to bring the ratio close to unity.

Table 1. SPSC Plasma Parameter Regimes

plasma density	$10^6 \le N_e \le 10^{12}$ cm^{-3}	
neutral density	$3 \times 10^{11} \le N_n \le 3 \times 10^{14}$ cm^{-3}	
electron temperature	$T_e \approx 0.5$ eV	
ion temperature	$T_i \approx 0.05$ eV	
Debye length	$0.5 \le \lambda_D \le .5 \times 10^{-4}$ cm	
electron plasma frequency	10 MHz$\le f_{pe} \le$ 300 MHz	
electron thermal speed	$V_{te} = 3 \times 10^7$ cm s^{-1}	
ion thermal speed	$V_{ti} = 5 \times 10^4$ cm s^{-1}	
ion acoustic speed	$Cs = 1.1 \times 10^5$ cm s^{-1}	
electron gyroradius	ρ_e = 0.16 cm (**B=10 G**)	0.04 cm (**B=40 G**)
electron gyrofrequency	f_{ce}=28 MHz (")	112 MHz (")
ion gyroradius	ρ_i = 14 cm (")	3.6 cm (")
ion gyrofrequency	f_{ci}=380 Hz (")	1.5 kHz (")
ion-neutral collision frequency	$0.03 \le \nu_{in}/\Omega_i \le 30$ (")	$0.01 \le \nu_{in}/\Omega_i \le 8$ (")
electron-neutral collision frequency	$4 \times 10^{-4} \le \nu_{en}/\Omega_e \le 0.07$ (")	$10^{-4} \le \nu_{en}/\Omega_e \le 0.02$ (")

Electronics: charging and discharging scenario

A typical cycle time for the experiment is ≤ 30 seconds. This includes capacitor charging, firing, discharging and data collection. The primary analysis routines are LABVIEW software-based and AD interfaces employ an array of CAMAC digitizers.

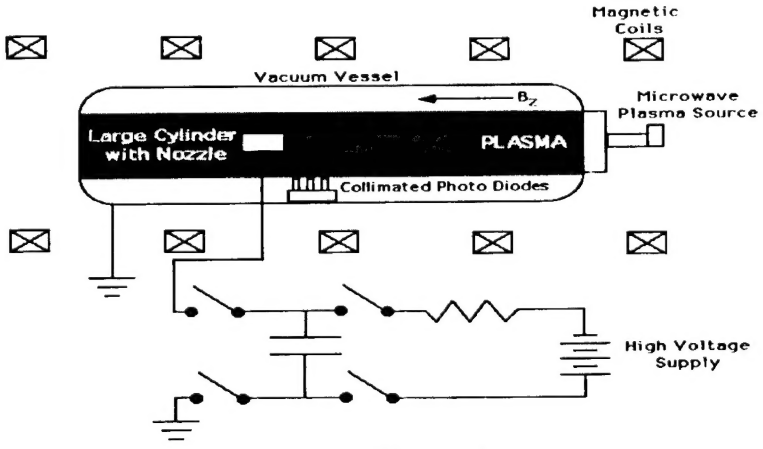

Figure 4

The SPEAR III program included testing of critical components in a 'mock-up' (as close to flight conditions as possible) configuration in the NASA-Lewis Research Center's, Plum Brook Station B2 vacuum facility. The mock-up had the advantage of allowing a direct measurement of the voltage difference between the payload body and the vacuum chamber wall. This was carried over into the NRL experiment. The charging electronics used in the laboratory testing for the SPEAR III program were brought to NRL, and the initial configuration was designed to first test neutral gas release effects from a single cylinder, as shown schematically in Figure 4. Also shown in Figure 4 are the relative positions of the light sensitive diodes used in an investigation of the dynamic sheath expansion during discharge. Details on the charging method can be found in papers relating to both the SPEAR I *[Allred et al., 1988; Katz et al., 1989]* and SPEAR III *[Mandel et al., 1998; Berg et al., 1995]* rocket experiments. For the mock-up and the flight experiments one side of a high-voltage capacitor on the payload was charged to +10 kV and the other side was connected through a relay to a large sphere deployed on a high-voltage boom. This configuration was chosen so that in a plasma with the characteristics of the normal F-region ionosphere the sphere/payload combination will float (with respect to the plasma) with at least -2 kV appearing on the payload with the remaining voltage appearing on the sphere. Thus, as the voltage on the capacitor decays, the payload voltage will go through the entire range of voltages normally associated with natural charging, i.e., 0 to -2 kV. A resistor across the charging capacitor allows for a 1 sec decay time of the voltage. Any current flowing through the plasma will shorten this decay time. During the experiments the decay time is typically between 0.3-1.0 sec, except when a large breakdown occurs and generates a high current discharge path. The capacitor is then discharged in milliseconds. For the rocket experiment the charge and decay cycle was set to repeat every 5 seconds. The SPSC testing was done on a single 'shot' basis where the charging and data-taking cycle was controlled manually.

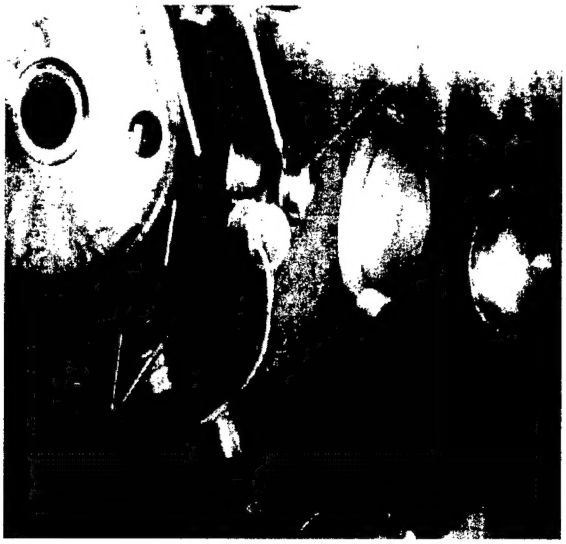

Figure 5

For the laboratory experiments the high voltage capacitor could be connected between two cylinders, or a single cylinder could be biased with respect to the chamber walls. For the experiment described here we chose the single cylinder configuration and applied voltages as high as -3 kV. In this manner, the initial SPSC experimentation eliminates the sphere and applies the charging voltage directly across the "payload". Discharging of the simulated payload in the SPSC depends on the current collection area available for ions. Shown in Figure 5 is the initial setup of the two-cylinder configuration in the laboratory, whereas Figure 4 shows the schematic representation of the initial one cylinder experimental arrangement. In the laboratory simulation the small cylinder in Figure 5 is removed from the experiment, a neutral gas release valve is placed in the large cylinder and kilovolt level charging occurs before release. The single aluminum cylinder, which is 10 cm in diameter and 10 cm in length and was mounted in the

center of the chamber is shown along with the enclosed puff valve system schematically in Figure 6a. The gas supply which provides the neutral gas release is fed to the plenum inside the cylinder through a 1/4 inch plastic line, also visible in Figure 6. The reservoir is connected to a solenoid valve so that when the valve is opened the gas flows through and into the throat of the supersonic nozzle. Two separate nozzles, shown in Figures 6b and 6c, have been tested so far and they are designed to produce mach numbers of Mach 3 and Mach 9. As mach number is related to the ratio of exit area to throat area (shown below), the separate nozzles, even though machined identically at the throat, have different lengths from throat to exit and thus diverge to different exit areas.

During the discharges, cylinder voltage and current collected by the cylinder were measured as functions of time. A typical data set is shown in Figure 7. For measurement purposes, several in-house-developed diagnostics were used including fast-sweep Langmuir probes *[Siefring et al., 1997b]* to measure electron temperature, emissive probes to measure plasma potential, photo diodes to monitor neutral excitation and double probes to monitor particle flow and electric field. In addition, a high voltage sensor *[Siefring et al., 1995]* was developed and used in the laboratory testing in the determination of potential at various positions in the plasma.

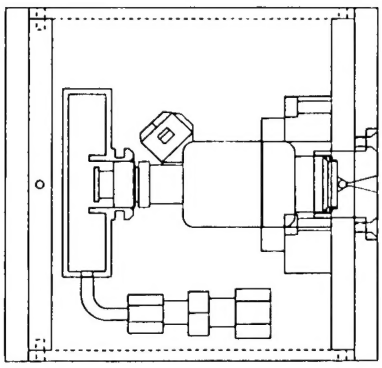

Figure 6a

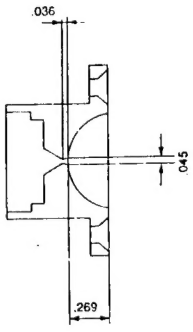

Figure 6b

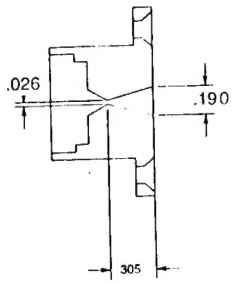

Figure 6c

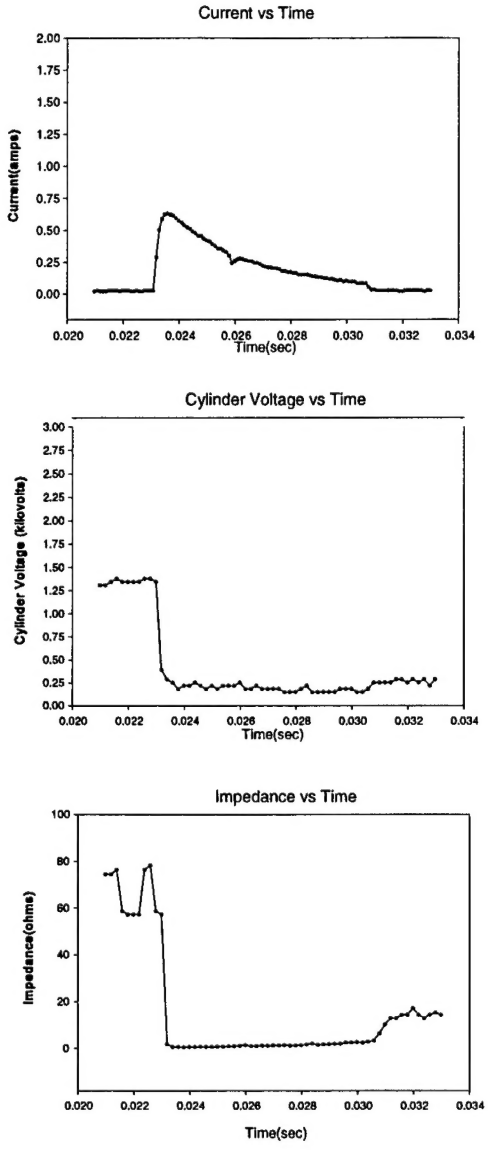

Figure 7

III. Experimental Results

In these studies we have done work related to the effects of NGR in a number of discharges where the voltage applied to the cylinder is varied from about -600 V to -2400 V. The gas valve is typically opened a short time ($\approx$10 ms) after charging and there is a subsequent local neutral pressure increase by several orders of magnitude in the near-space of the release valve. The discharge is initiated and the cylinder voltage falls to approximately -200 V as the collected current rises to the series resistor-limited value of about 1 amp. This behavior is seen in the first two plots of Figure 7 above.

It should be noted that the abrupt rise in the cylinder voltage near 0.036 sec is an artifact and not an important physical effect. Also, much of the accompanying experimental noise has been filtered from this data. As the gas breakdown process continues, electrons are accelerated away from the cylinder and ions are collected. Secondary electrons are created and also accelerated away from the cylinder creating further neutral excitation and other electron-ion pairs. The light emission caused by this excitation of the neutrals was monitored by an array of photo-diodes arranged in increasing distances from the discharge region, as seen schematically in Figure 4. The placement of these detectors is the first stage in determining expanding sheath characteristics during the discharge. Typical traces of this light intensity as a function of time and diode number are shown in Figure 8 with the intensity seen to fall off as a function of distance. The use of band pass filters over the photodiode demonstrates that the photons result primarily from neutral collisions.

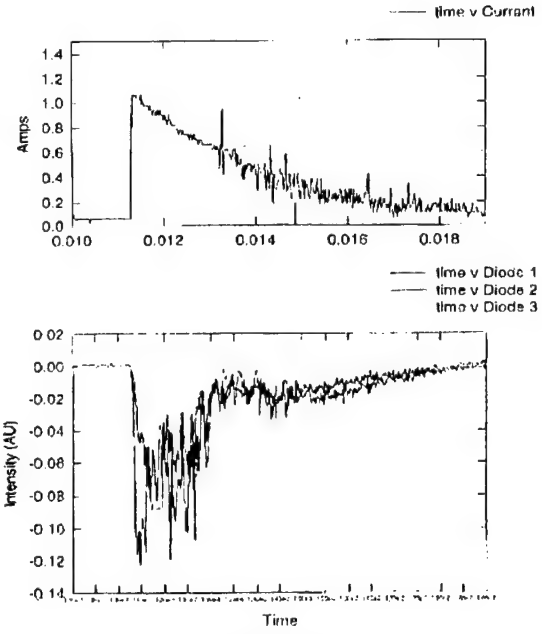

Figure 8

In Figure 9 the electron temperature measurements as a function of pulse duration on each of three probes at varying axial positions from the discharge region show enhanced electron temperature at the farthest probe position. This enhancement is consistent with the falloff in neutral density and the inelastic cooling rate of the electrons. The discharge duration is typically bounded initially by the release of neutral gas and finally by the decrease of potential below the minimum necessary to sustain ionization. The gas puff duration is significantly longer than the discharge time.

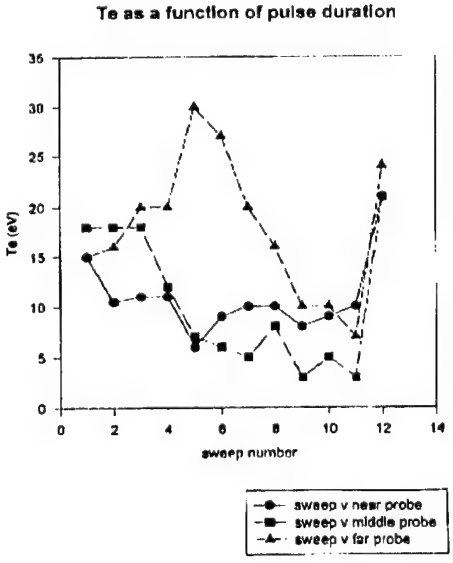

Figure 9

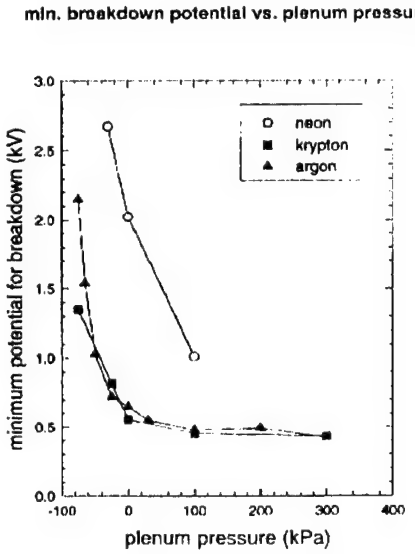

Figure 10

Figure 10 is a plot of the minimum potential necessary to initiate breakdown versus plenum pressure for three separate

gas puff species at a single fixed mach 9. Each point in Figure 10 corresponds to an average of 10 separate experimental runs. From this plot one can conclude that krypton and argon initiate breakdown at a lower potential than neon for the same gas plenum pressure, suggesting that perhaps heavier neutral gases initiate breakdown at lower potentials (See, however, the sections on theory and comparison to experiment below). Recent models *[Langely et al., 1984; Dietz and Sheffield, 1975]* allude to a velocity dependence on secondary electron emission that would seem to favor lighter gases. In Section IV we present a breakdown theory which addresses these possibilities and describes the data fairly well. We are in the process of building on the initial study by investigating the effectiveness of other gas species for mitigation of spacecraft charging.

With a goal toward minimizing gas usage, and therefore storage, we have studied the breakdown characteristics versus puff gas flow rate. Figures 11 and 12 show photographs of the discharges in argon and neon for the mach 3 and mach 9 nozzles separately. In general, the discharge appears more elongated for the higher mach number.

Argon puff

Figure 11

Neon puff

Figure 12

Figure 13 shows initial results of the discharge studies for Argon only. Each data point is again an average of 10 separate shots. The preliminary conclusion from this data is that the mach 9 nozzle valve discharges the cylinder at lower potentials than the mach 3 valve. We are preparing further experimentation in this area with a wider combination of release gases and valves.

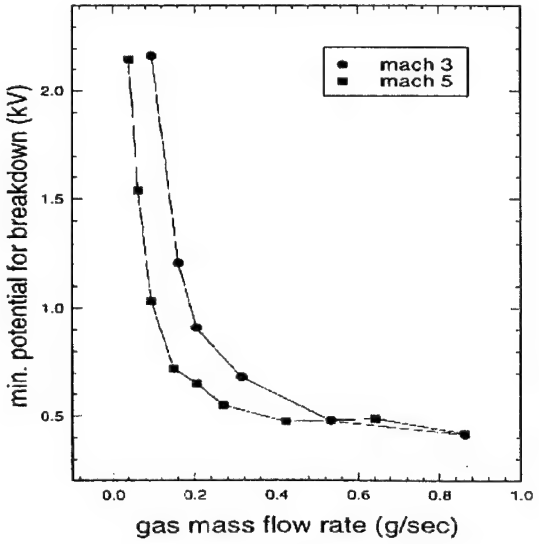

Figure 13

IV. Theory

The Discharge Model

The study of neutral gas breakdown in the presence of high potentials has been underway since the beginning of this century [*Townsend, 1900, 1901; Loeb, 1939; Raizer, 1997*]. The fundamental assumption is that the number of electrons grows exponentially in an avalanche fashion as one proceeds from cathode toward anode:

$$N(x) = N_0 \exp[\int_0^x \alpha(x)dx] \tag{1}$$

where N_0 is the number of electrons released from the cathode and α is the Townsend ionization coefficient and is defined as the number of ionization events performed along a 1 cm path in the electric field direction. Equivalently,

$$\alpha = \frac{\nu_i}{\nu_d} \tag{2}$$

with ν_i the ionization frequency and ν_d the electron drift speed. α is therefore a function of the neutral density (or pressure) and the electric field. An empirical formula for α ,

$$\alpha = A_1 N e^{-\frac{A_2 N}{E}} \tag{3}$$

is used in much of the theoretical and numerical analysis. Here A_1 and A_2 are determined from the experimental data for a particular gas and N is the neutral gas density. (We note here that often this expression is given in terms of neutral gas pressure. This causes complications, however, when temperature varies and the usual standard room temperature is not the applicable temperature. To use pressure in the conventional sense one has to make the distinction that the pressure given is related to the neutral density through standard room temperature, and, in any case, this is confusing. For this reason we prefer to express the relation through N.) For inert gases, however, a better fit to the experimental data is provided by *Raizer, [1997]*,

$$\alpha = B_1 N e^{-B_2 (\frac{N}{E})^{\frac{1}{2}}} \quad (4)$$

where B_1 and B_2 are empirical "constants" determined from the ionization curves.

The condition for a self-sustaining discharge *[Raizer, 1997]* is,

$$I = \int_0^\infty dx \ \alpha(x) \geq \ln(1+\gamma_i^{-1}) \quad (5)$$

where γ_i is the coefficient for electron emission from the cathode per incident ion. For $\gamma_i \sim 0.15$, for example, the right hand side of this equation equals 2. The minimum voltage should be 100 V or more, based on the data for Townsend discharges (space-charge free) and glow discharges (with space charge). At this voltage, the gas density, N, times the gap separation, d, ranges from 7×10^{15} to 5×10^{16} cm^{-2}, depending on the gas, the cathode material and the spatial profile of E/N. At higher or lower values of Nd, larger voltages are needed to produce breakdown. This suggests that a gas puff can discharge an object of characteristic radius R, provided it is charged (negatively) to a few hundred volts or more and NR lies between 7×10^{15} and 5×10^{16} cm^{-2}. Here N is the gas density averaged over R. In the present experiments, R~ 10 cm, which suggests that the optimal value of N lies between 10^{15} and 10^{16} cm^{-3}. Such densities are achievable, according to the analysis below. Note that the density required varies inversely with the size, R, of the object.

Analysis of Eqs (4) and (5) shows that the minimum voltage for breakdown, ϕ_{min}, occurs near the peak of the ionization curve, where $\alpha/N = (\alpha/N)_{max}$ and $E/N = (E/N)_{min}$. Setting $(E/N)_{min} = \phi_{min}/NR$ and $\alpha_{max}R$ equal to $\ln(1+\gamma_i^{-1})$ based on condition (2), we obtain

$\phi_{min} \approx [(E/N)_{min}/(\alpha/N)_{max}] \ln(1+\gamma_i^{-1})$. In noble gases $(\alpha/N)_{max} \sim 3 \times 10^{-16}$ cm^2 and $(E/N)_{min} \sim 3 \times 10^{-14}$ V-cm^2. The minimum breakdown voltage is then $\phi_{min} \sim 100 \ln(1+\gamma_i^{-1}) \sim 200$ V. Note that ϕ_{min} scales directly with the right hand side of Eq. (5). It might be noted that this voltage is roughly an order of magnitude smaller than the minimum voltage for self-sustained streamers as given by *Raether, [1939]*

Neutral Gas Release (NGR) - Description of the Expansion

Equations (3) and (5) indicate that two parameters determine whether breakdown occurs for a particular gas. The first is the field profile, E(z), which is determined by the charging voltage and system geometry. The other is the gas-density profile, $N(z) = F_0/v(z)A(z)$, where F_0 is the total flux, v(z) is the local flow velocity, and A(z) is the local transverse area of the gas

puff. We compute F_0, v(z) and A(z), relying in part on the early work *of Barrere, [1960]*. Consistent with this approach, we assume isentropic expansion and isotropic temperature along z. In addition we point out some applicable features associated with definition of nozzle mach number.

(i) No nozzle: Free expansion of an ideal gas

Consider a large pressurized box with a small hole in one side. Particles inside are assumed to have a Maxwellian velocity distribution, and only those with $v_z > 0$ can escape through the hole. If the expansion is into complete vacuum, then the mean forward velocity is given by,

$$\langle v_z \rangle = \frac{\int_0^\infty dv_z v_z e^{\frac{-mv_z^2}{2T_c}}}{\int_0^\infty dv_z e^{\frac{-mv_z^2}{2T_c}}} = \sqrt{\frac{2T_c}{\pi m}} \qquad \textbf{(6)}$$

where T_c is the chamber temperature and m is the molecular mass. The mean forward speed is thus less than $0.7v_s$, where $v_s = (\gamma T_c/m)^{1/2}$ is the sound speed and $\gamma \geq 1.2$ is the adiabatic constant. In passing through the hole the transverse temperature is unchanged, $T_\perp = T_c$, while the longitudinal temperature falls to $T_z = \langle mv_z^2 \rangle - m\langle v_z \rangle^2 = (1-2/\pi)T_c \approx 0.36\, T_c$. Gas collisions will eventually restore temperature isotropy and in a noble gas T_z and $T_\perp$ approach $0.8\, T_c$. Thus only twenty percent or so of the initial thermal energy is realized as forward energy.

(ii) Expansion with nozzles

However a much higher conversion efficiency is obtainable using a gas nozzle. In a nozzle the flow is primarily one dimensional through an area which varies with distance. The area first constricts to a minimum at the throat where the flow speed becomes the local sound speed, $v_t = (\gamma T_t/m)^{1/2}$ where $T_t = (2/\gamma+1)T_c$ is the gas temperature at the throat. Past the throat the nozzle area again increases as can be seen in the nozzle diagrams of Figure 6. Using part of the analysis by *Barrere [1960, Ch. 2]*, we can show that the nozzle area A and velocity v are related to the values at the throat by,

$$\frac{A_t}{A} = \frac{v}{v_t}\left[\left(\frac{\gamma+1}{2}\right)\left(1-\left(\frac{\gamma-1}{\gamma+1}\right)\left(\frac{v}{v_t}\right)^2\right)\right]^{\frac{1}{\gamma-1}} \quad (7)$$

This equation indicates that v/v_t is double valued for a given value of A. This relation is plotted in Figure 14 which shows that in the constricting region before the throat , $v<v_t$; and in the expanding region after the throat, $v > v_t$. The velocity thus rises as the nozzle constricts and as it expands. The velocity at the nozzle exit depends on the final area ratio but is always limited (for $A \to \infty$) to

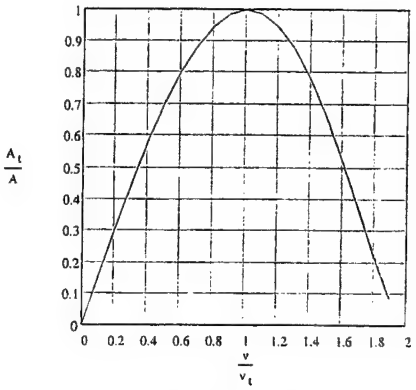

Figure 14

$$v_e \le v_{max} = \sqrt{\frac{\gamma+1}{\gamma-1}}v_t = \sqrt{\frac{2}{\gamma-1}}v_s \quad (8)$$

Nozzle mach numbers are typically quoted by using the ratio of v_e to the local sound speed, c_{sl}, at nozzle exit or,

$$M \equiv \frac{v_e}{c_{sl}} = \frac{v_e}{c_s}\sqrt{\frac{T_c}{T_e}} = \left(\frac{v_e}{c_s}\right)^{\frac{2\gamma-1}{2(\gamma-1)}}\left[\frac{A_e}{\Gamma' A_t}\right]^{\frac{1}{2(\gamma+1)}} \quad (9)$$

Here A_e is the exit area and T_e is the exit temperature which we can find from,

$$\frac{T_e}{T_c} = \frac{2}{1+\gamma}\left[\frac{A_t}{A_e}\frac{v_t}{v_e}\right]^{\gamma-1} \quad (10)$$

where the coefficient Γ' is given by,

$$\Gamma' = \left[\frac{2}{\gamma+1}\right]^{\frac{\gamma+1}{2(\gamma-1)}} \quad (11)$$

The flow rate F_0 equals the mass flow rate divided by the molecular mass, m. Alternatively, F_0 can be computed from the chamber pressure p_c and the throat area A_t using,

$$F_0 = \Gamma \frac{p_c A_t}{\sqrt{mT_c}}, \quad where\ \Gamma = \sqrt{\gamma}\Gamma' \tag{12}$$

(iii)Expansion after leaving nozzle

We next determine the velocity v(z) and the area A(z) outside the nozzle. Because there is residual energy in the gas, the expansion accelerates longitudinally and transversely. The longitudinal acceleration is negligible, however, because the exit temperature is small compared with the chamber temperature, $T_e << T_c$. For example, for the M3 nozzle, $T_e/T_c = 0.05$ according to Eq. (10); for the Mach 9 nozzle this ratio is even smaller. Therefore, past the nozzle it is legitimate to approximate $v(z) \sim v_e$.

Transverse acceleration is generally small as well. To show this, we observe that the gas can be treated as a jet moving with a fixed longitudinal speed, v_e, outside the nozzle. Since the transverse velocity is presumed small, $v_\perp << v_e$, the jet can be treated as a freely expanding, long beam. In that case the area expands as *[Fernsler et al., 1994]*

$$A(z) = A_e + 2z\sqrt{\pi A_e}\ \tan\theta_0 + \pi z^2[\tan^2\theta_0 + \frac{2T_e}{mv_e^2}] \tag{13}$$

where $\theta_0 = v_\perp/v_e$ at z=0 is the half-angle of the nozzle. . This expansion produces a larger area at a given z than simple cylindrical expansions due to the presence of thermal energy.

V. Comparisons of Theory and Experiment

Breakdown potentials versus gas flow

Using the criterion outlined in Eq (5) above we plot in Figures 15 through 17 the predicted breakdown voltages for the three gases used in the experiment and for each of the two nozzles. The plot of Figure 15 also shows the argon data superimposed on the theoretical plots. From these plots, the lightest gas tested, neon (Figure 17), requires significantly higher levels of release gas to break down for a given cylinder charging voltage than either argon or krypton.

This result is consistent with the data shown in Figure 10 where breakdown potential versus plenum pressure is plotted for each of the three release gases using the mach 9 nozzle.

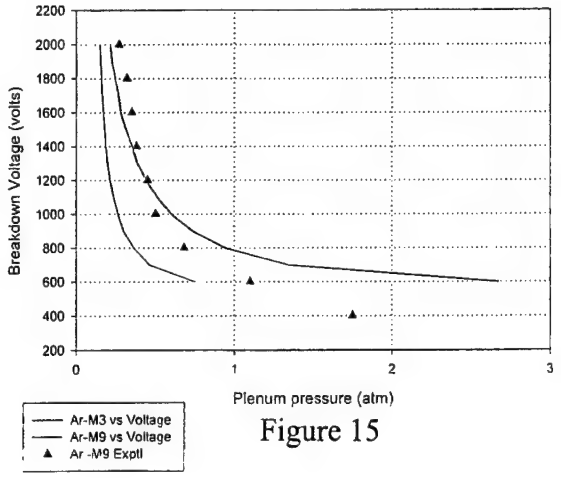

Figure 15

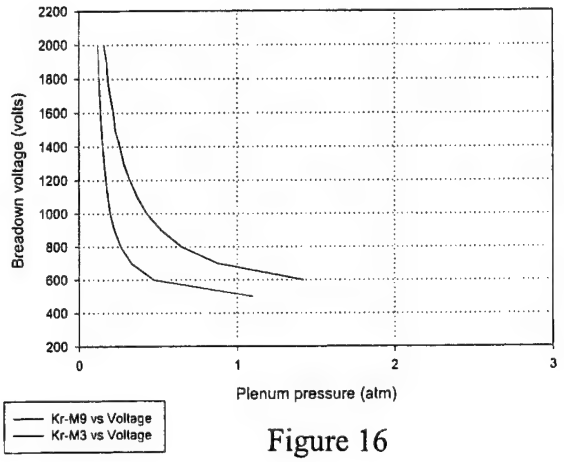

Figure 16

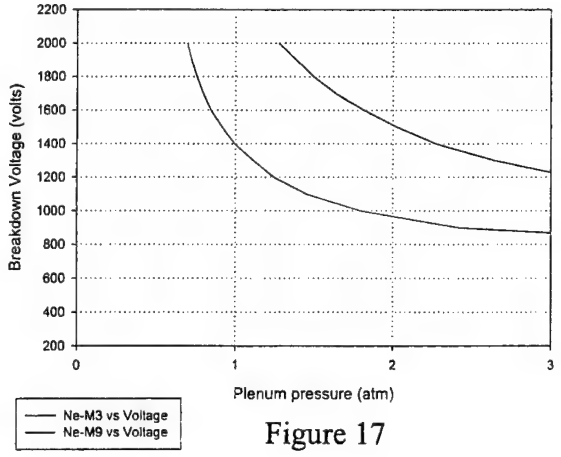

Figure 17

If we examine the breakdown condition of Eq.(5) in somewhat more detail the integral appears as,

$$I = \int_{z_L}^{\infty} N(z,p) c_1 e^{\frac{-c_2}{\sqrt{\frac{E(z)}{N(z,p)}}}} dz \qquad \textbf{(14)}$$

where N(z,p) is neutral density given by,

$$N(z,p) = \frac{F_0(p)}{A(z)v_e} , \qquad \textbf{(15)}$$

and z_L is the lower integration limit. $F_0(p)$ is the conserved neutral particle flux from the plenum, A(z) is as given in Eq. (13) and v_e is the exit velocity which is calculated from the area ratio of Eq. (7). This relation assumes that the velocity of the exit gas is constant as a function of distance from the release point. We note specifically that z_L corresponds to the surface of the charged object where spherical symmetry is assumed, *i.e.*, z = 0 is taken as the origin of a charged sphere for definition of the spatial falloff of the potential. In this analysis then, the electric field and potential have the simple one-dimensional form,

$$\Phi(z) = -V_{ch}(\frac{z_L}{z}) \qquad \therefore \quad E(z) = V_{ch}(\frac{z_L}{z^2}) \qquad \textbf{(16)}$$

where V_{ch} is the charging potential. With the definition of z_L as above, we are assuming that the exit area of the nozzle is at the surface of the cylinder; therefore $A(z_L)$ corresponds to A_e in Eq. (7) and $N(z_L,p)$ is the gas density at the exit area face (note, not the throat). $F_0(p)$ is dependent upon the pressure, p, and temperature, T, in the plenum, the release gas molecular mass, μ, and the area of the nozzle throat, A_t , *i.e.*,

$$F_0(p) = \Gamma \frac{p\ A_t}{\sqrt{mRT}} \qquad \textbf{(17)}$$

In this equation, the molecular mass, m, is in kg, p in pascals, A_t in m^2, T in Kelvin, Γ is defined in Eq. (12), and R is the universal gas constant.

Breakdown dependence on release gas mass

Since the density, as seen in Eq. (15), appears in the breakdown integral Eq. (14) both as a multiplicative factor and also in the exponent under a square root, it is not immediately obvious what overall effect an increase of mass produces without numerical evaluation of the integral as we have done here. In fact, however, we can show that $N_{cm}(z,p)$ is independent of the release gas mass and therefore that the breakdown integral of Eq. (15) is largely determined by the ionization coefficients for the various gases; therefore, although the breakdown is dependent upon the gas species through these coefficients, it is not a function of the mass. In fact we can show,

$$N(z) = \frac{A_e}{A(z)} N_e \tag{18}$$

where N_e is the gas density at nozzle exit and is related to density in the chamber through,

$$N_e = \left(\frac{T_e}{T_c}\right)^{\frac{1}{\gamma-1}} N_c \tag{19}$$

Eq (18) results from simple flux conservation and the assumption of (nearly) constant flow velocity outside the nozzle. Eq. (19) arises from Eqs. (6) and (7) and the relation between velocity in the nozzle throat and sound speed in the plenum,

$$v_t = \sqrt{\frac{2}{\gamma+1}} v_s \tag{20}$$

The independence of density and therefore of breakdown on gas mass is apparently the explanation of the experimental result shown in Figure 10 that the breakdown potential gas flow requirement for krypton and argon is similar whereas the difference between these two and neon is substantial. This occurs even though there is approximately a factor of two mass difference between each mass and so, at first glance, one might be inclined to guess a more or less linear dependence on release gas mass. As covered above, this dependence is largely a function of the ionization curves for the different species and not the mass.

Breakdown dependence on release-gas mach number

As demonstrated above the gas density at a fixed distance from the nozzle is independent of mass; however, not of exit velocity and therefore (local) mach number as seen in Eq.(15). Since the variation of pressure in the plenum is essentially an isothermal process there is no effect on the gas exit velocities from this variation. There is only an adjustment in gas density which occurs with varying plenum pressure. At a fixed pressure and fixed distance from the nozzle therefore, we plot the density dependence on the ratio of exit velocities in Figure 18. We see that as the exit area increases (or as the local mach number or velocity ratio increases) the density decreases. Although not shown the density continues to decrease to the point that at the limit that the velocity ratio is 2, we produce an infinite area and hence a density decrease to zero. Figure 19 shows a plot of the breakdown integral as a function of the velocity ratio for neon at a fixed position and pressure. The value of the breakdown integral is seen to be a monotonic function of the velocity ratio, and hence of the valve mach number, up until, the limit of infinite area where the function decreases. This occurs because of the steep decline in the gas density levels beyond a certain distance from the nozzle. These theoretical arguments would then suggest that the higher mach number nozzles should produce breakdown with less gas pressure than lower mach number nozzles. These results are corroborated by the experimental plots as pointed out above.

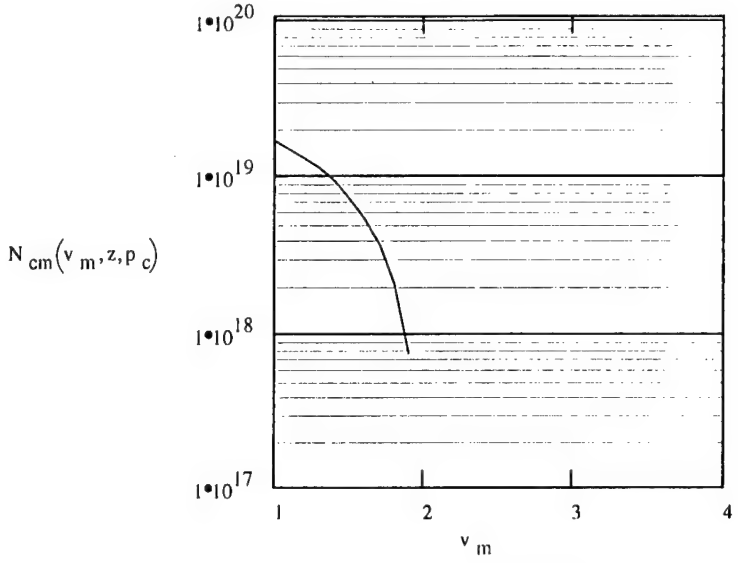

Figure 18

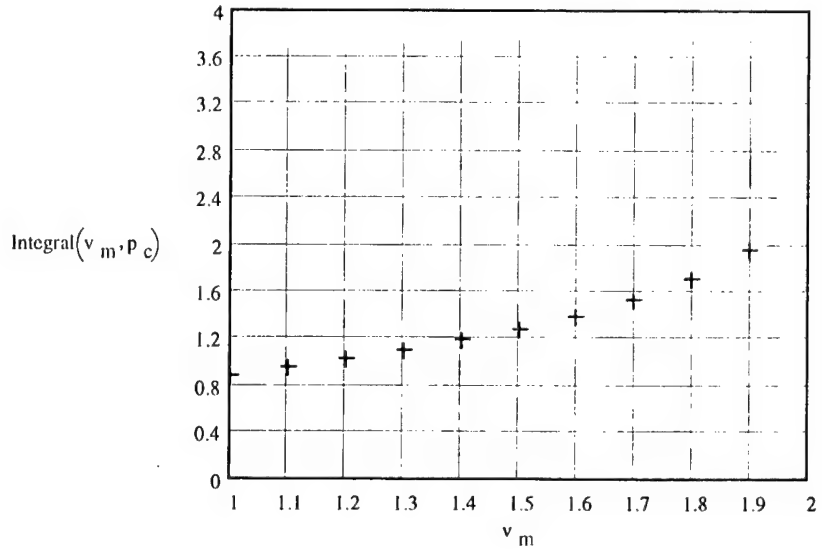

Figure 19

VI. Summary

We have conducted preliminary laboratory simulations and developed a basic theoretical model of the effects of neutral gas release on space vehicle charging in the LEO space environment. The experiments were performed in the NRL Space Physics Simulation Chamber.

The results presented here are the first stage of a more exhaustive investigation into the optimum choice of a release gas and release speed in order that spacecraft which acquire potentials either through natural or artificial means can discharge these voltages at the lowest level possible. The Townsend discharge model and breakdown criterion expressed through the integral of Eq (5) explain and predict the experimental results quite well. Because of the success of this model we are in the process of continuing work with it in order to guide certain phases of the experimental effort and to suggest nozzle and gas release designs for optimum performance.

At the present stage of the experiment we are able to conclude that argon and krypton tend to discharge the payload at lower potential than neon and that the higher mach number (M9) valve also is better at discharging for a given plenum pressure than the lower mach number valve (M3). We are continuing this experiment with studies using different neutral gases and mixtures of neutral gases, with different cylinder surfaces and with varying electron and neutral gas environments. In addition we are investigating the effect of the orientation of the puff with respect to the local magnetic field.

Acknowledgment:

We gratefully acknowledge the support of the Office of Naval Research. In addition, the Ballistic Missile Defense Organization (BMDO) was responsible for early support in the SPEAR effort from which much of the pulsing electronics was derived.

VII. Figure Captions

Figure 1. A schematic diagram of the NRL Space Physics Simulation Chamber showing diagnostic equipment

Figure 2. A photograph of the NRL SPSC facility.

Figure 3. A photograph of the wide-area microwave plasma source showing magnetron and coupling wave guides.

Figure 4. A schematic diagram of the charging electronics and cylinder/nozzle inside the SPSC

Figure 5. A photograph of the the two-cylinder charging arrangement inside the SPSC

Figure 6. Engineering drawings of a. the charged cylinder with cut-away view of gas plenum and nozzle, b. the mach 3 nozzle, c. the mach 9 nozzle.

Figure 7. Plots of experimental collected current, cylinder voltage and impedance as a function of time during a discharge.

Figure 8. Experimental traces of current collection and light intensity as measured by diodes at varying distances from the cylinder during discharge

Figure 9. Experimental electron temperature as measured by Langmuir probe sweeps at varying distances from the cylinder as a function of pulse duration.

Figure 10. Experimental plots of minimum potential necessary for breakdown for each of three gases as a function of plenum pressure. Mach 9 (M9) nozzle.

Figure 11. A photograph of an argon gas puff (M3 nozzle)during discharge.

Figure 12. A photograph of a neon gas puff (M9 nozzle) during discharge

Figure 13. Experimental plots of minimum potential necessary for breakdown for each of the two nozzles, M3 and M9 as a function of gas mass flow rate.

Figure 14. A theoretical plot of the ratio of nozzle throat area to exit area versus ratio of exit velocity to sound speed in nozzle throat. This theoretical relation is plotted from Eq. (7).

Figure 15. A theoretical plot of minimum breakdown voltage versus plenum pressure for argon with two different nozzles, M3 and M9. Experimental breakdown for the M9 nozzle is plotted as triangles for comparison. As derived from the breakdown integral criterion of Eq (5).

Figure 16. A theoretical plot of breakdown voltage versus plenum pressure for krypton with two different nozzles, M3 and M9.As derived from the breakdown integral criterion of Eq (5).

Figure 17. A theoretical plot of breakdown voltage versus plenum pressure for neon with two different nozzles, M3 and M9. As derived from the breakdown integral criterion of Eq (5).

Figure 18. A theoretical plot of neon neutral gas density (Eq. (15)) at fixed distance from the cylinder and constant pressure versus release gas mach number.

Figure 19. A theoretical plot of the results of the the breakdown integral criterion of Eq. (5) at fixed distance from the cylinder and constant pressure versus release gas mach number

VIII. References

Allred, D.B., D.B., J.D. Benson, H. A. Cohen, W. J. Raitt, D. A. Burt, I. Katz, G. A. Jongeward, J.Antoniades, M. Alport, D. Boyd, W. C. Nunnally, W. Dillion, J. Pickett, and R. B. Torbert, The SPEAR-I experiment: High voltage effects on space charging in the ionosphere, ***IEEE Trans. on Nucl. Sci., 35***, 1386, 1988.

Alport, M.J., J.A. Antoniades, D.A. Boyd, R.G. Greaves, and R.F. Ellis, Electrical Breakdown at Low Pressure in the presence of a weak magnetic field, ***J. Geophys. Res., 95***, 6145, 1990

Amatucci, W.E., M.E. Koepke, J.J. Carroll III and T.E. Sheridan, Observation of ion-cyclotron turbulence at small values of magnetic field aligned current, ***Geophys. Res. Lett., 21***, 1595, 1994

Amatucci, W.E., D. N. Walker, G. Ganguli, J. A. Antoniades, D. Duncan, J. H. Bowles, V. Gavrishchaka, and M. E. Koepke, Plasma response to strongly sheared flow, ***Phys. Rev. Lett.***, 77, 1978 (1996).

Amatucci, W.E., D. N. Walker, G. Ganguli, D. Duncan, J. A. Antoniades, J. H. Bowles, V. Gavrishchaka, and M. E. Koepke, Velocity-shear-driven Ion-Cylcotron waves and associated transverse ion heating, submitted ***J. Geophys. Res.***, to appear in June 98 issue, 1998a

Amatucci, W.E., G. Ganguli, D.N. Walker, D. Duncan, ***Phys. Rev. Lett.***, Space Chamber Simulation of Ion Heating in the Low-Altitude Ionosphere: A Comparison of Wave and Joule Heating Mechanisms, in review, submitted 1/98, 1998b

Barrere, M., A. Jaumotte, B. Fraeijis De Veubeke, J. Vandenkerckhove, ***Rocket Propulsion***, Elsevier Publishing Co., 1960

Benjamin, N., High-impedance capacitive divider probe for potential measurements in plasmas,***Rev. Sci Instrum., 53***, (10), 1541, 1982.

Berg, G.A., W.J. Raitt, D.C Thompson, B.E. Gilchrist, N.B. Myers, P. Rodriguez, C.L. Siefring, H.R. Anderson and D.W. Potter, Overview of the effects of neutral gas releases on high-voltage sounding rocket platforms, ***Adv. Space Res., 15***, (12)83, 1995

Block, L.P. and C.-G. Faelthammar, The role of magnetic-field-aligned electric fields in auroral

acceleration, ***J. Geophys. Res., 95***, 5877, 1990

Borovsky, J. E., The dynamic sheath: Objects coupling to plasmas on electron-plasma-frequency time scales, ***Phys. Fluids, 31***, 1074, 1988.

Bowles, J.H., D. Duncan, D.N. Walker, W.A. Amatucci and J.A. Antoniades, A Large Volume Microwave Plasma Source, ***Rev. Sci. Instr., 67***, 455, 1996

Dietz, l.A. and j.C. Sheffield, ***J. Appl. Phys., 46***, 4361, 1975

Fahleson, U.V., Theory of electric field measurements conducted in the magnetosphere with electric probes, ***Space Sci. Rev.,*** *7*, 238, 1967.

Fernsler, R.F., R.F. Hubbard and M. Lampe, Long-range propagation of high-power, pulsed electron beams for welding and materials applications, ***J. Appl. Phys., 75***, 3278, 1994

Garret, H.B., The charging of spacecraft surfaces, ***Rev. Geophysics, 19,*** 577, 1981.

Gilchrist, B.E., P.M. Banks, T. Neubert, P.R. Williamson, N.B. Meyers, W.J. Raitt, and S. Sasaki, Electron collection enhancement arising from neutral gas jets on a charged vehicle in the ionosphere, ***J. Geophys. Res., 95***, 2469, 1990

Gilchrist, B.E., P.M. Banks, T. Neubert, C. Bonifazi, D.C. Thompson, W.J. Raitt, and S.D. Williams, Modification of the TSS 1 electrodynamic tether current-voltage characteristics due to orbiter thruster firings, ***Eos Trans. AGU, 74***, (43), Fall Meeting Suppl., 466, 1993

Greaves, R.G., D.A. Boyd, J.A. Antoniades and R.F. Ellis, Steady state Toroidal Plasma around a spherical anode in a magnetic field, ***Phys. Rev. Lett., 64(8),*** 886, 1990

Gussenhoven, M.S., D. A. Hardy, F. Rich, W. J. Burk, and H. C. Yen, High-level spacecraft charging in the low-altitude polar auroral environment, ***J. Geophys. Res., 90***, 11,009, 1985.

Hastings, D.E., M. Cho, and H. Kuninaka, The arcing rate for a high voltage solar array: theory,

experiments and predictions, ***Journal of Spacecraft and Rockets, 29***, 538, 1992.

Katsumata, I. And M. Okazaki, Ion sensitive probe-A new diagnostic method for plasmas in magnetic fields., ***Jpn. J. Appl. Phys., 6*** ,123, 1967

Katz, I., G. A. Jongeward, V. A. Davis, M. J. Mandell, R. A. Kuharski, J. R. Lilley, Jr., W. J.Raitt, D. L. Cooke, R. B. Torbert, G. Larson, and D. Rau, Structure of the bipolar plasma sheath generated by SPEAR I, ***J. Geophys. Res., 94***, 1450, 1989

Kaufmann, R.L., D. N. Walker, J. C. Holmes, C. J. Pollock, R. L. Arnoldy, L. J. CaHill and P.Kintner, P.M., Heavy ion beam-ionosphere interactions: charging and neutralizing the payload, ***J. Geophys. Res., 94***, 453, 1989.

Kennerud, K.L., High Voltage solar array experiments, ***Boeing Co., Seattle***, 1974, NASA cR121280.

Koons, H.C., P. F. Mizera, J. L. Roeder and J. F. Fennel. Severe spacecraft-charging event on SCATHA in September 1982, ***J. Spacecr. and Rockets, 25***, 239-243, 1988.

Langley, R.A., ***J. Plasma Phys. Thermonucl. Fus., Special Issue***, 99, 1984

Langmuir, I. and K. B. Blodgett, Current limited by space charge flow between conducting spheres, ***Phys. Rev., 74***, 49, 1924.

Loeb, L.B., ***Fundamental Processes of Electrical Discharge in Gases***, Wiley, New York, 1939

Machuzak, J.S., W.J. Burke, L.C. Gentile, V.A. Davis, D.A. Hardy, and C.Y. Huang, Thruster effects on the Shuttle potential during TSS 1, ***J. Geophys. Res., 101***, 13,347, 1996

Mandel, M.J., G.A. Jongeward, D.L. Cooke and W.J. Raitt, SPEAR 3 flight analysis: Grounding by neutral gas release, and magnetic field effects on current distribution, ***J. Geophys. Res., 103***, 439, 1998

McCoy, J.E. and Konradi, A., Sheath Effects observed on a 10-meter high voltage panel in

simulated low earth orbit plasma, ***Proc. Spacecraft Charging Technology Conference, Air Force Academy***, Colo. Springs, CO., 1978, NASA CP-2071

McPherson, D.A., D. P. Cauffman and W. Schober, Spacecraft charging at high-altitudes-The SCATHA satellite program, ***The 13th Aerospace Science Meeting, Am. Inst. of Aeronaut. Astronaut.***, Pasadena, Calif., 20-22, 1975.

McPherson, D.A., and W.R. Schober, Spacecraft charging at high altitudes: The SCATHA satellite program, Spacecraft Charging by Magnetospheric Plasmas, edited by A. Rosen, ***Progr. Aeronaut. Astronaut., 47***, 15-30, 1976.

Mullen, E.G., M. S. Gussenhoven, D. A. Hardy, T. G. Aggson, B. G. Ledley, E. Whipple, SCATHA survey of high-level spacecraft charging in sunlight, ***J. Geophys. Res., 91***, 1474, 1986.

Neubert, T., M. J. Mandell, S. Sasaki, B. E. Gilchrist, P. M. Banks, P. R. Willimson, W. J.Raitt, N. B. Meyers, K. I. Oyama, and I. Katz, The sheath structure around a negatively charged rocket payload, ***J. Geophys. Res., 95***, 6155, 1990

Olsen, R.C., R.C., L. E. Weddle and J. L. Roeder, Plasma wave observations during ion gun experiments, ***J. Geophys. Res., 95***, 7759, 1990.

Pongratz, M.B., D. Walker, M. Baumback, C. Siefring, H. Anderson, D. Potter, Plasma Physics Instrumentation, ***BEAR (Beam Experiments Aboard a Rocket) Project Final Report, Volume II: Flight Results and System Evaluation***, G.J. Nunz, A.D. McGuire, P.G. O'Shea, E. B. Barnett, editors, Los Alamos National Laboratory, LA-11737-MS, Vol II, Part I, BEAR-DT-7-2, pp 7-1 to 7-65, 1991

Raether, H., ***Zeitschrift fuer Physik. 112***, 464, 1939

Raizer, Y.P., ***Gas Discharge Physics***, Springer-Verlag, Berlin, 1997

Roth, I.C.,. C. W. Carlson, M. K. Hudson, and R. L Lysak, Simulations of beam excited minospecies gyroharmonics in the porcupine experiment, ***J. Geophys. Res., 88***, 357, 1983.

Siefring, C.L., P. Rodriguez, M.M. Baumback, J.A. Antoniades, and D.N. Walker, A method for measuring large changes in the payload potential of rockets and satellites, ***Rev. Sci. Instrum., 66***, 4681, 1995

Siefring, C. L., and P. Rodriguez, Results from the NRL floating probe on SPEAR III: High time resolution measurements of payload potential, accepted ***J. Geophys. Res. Monograph***, 1997a

Siefring, C.L., W.E. Amatucci, and P. Rodriguez, Fast electron temperature measurements with Langmuir probes: Considerations for space flight and initial laboratory tests, accepted, ***J. Geophys. Res. Monograph***, 1997b

Stevens, N.J., Solar array experiments on the SPHINX satellite, ***NASA TMX-71458***, 1973

Stevens, N.J., Spacecraft system charged particle environmental interactions, ***Proc. Spacecraft Charging Technology Conference, Air Force Academy***, Colo. Springs, CO, Oct 1978 (NASA CP-2071)

Thiemann, I. And K. Bogus, Anomalous current collection and arcing of solar-cell modules in a simulated high-density low earth orbit plasma, ***ESA Journal, 10***, 43, 1986

Townsend, J.S., ***Nature, 62***, 340, 1900;

Townsend, J.S., ***Phil. Mag., 1***, 198, 1901

Walker, D.N., D. Duncan, J.A. Stracka, J.H. Bowles, C. L. Siefring, M.M. Baumback and P. Rodriguez, A tunable microwave source for space plasma simulation experiments, ***Rev. Sci. Instr., 65***, 661, 1994

Walker, D.N., J. Chen, J. Bowles, D. Holland, C. Siefring, D. Duncan, J. Stracka, and J. Antoniades, Nonlinear Particle Dynamics in the Magnetotail: A Laboratory Study 1. The Experimental Configuration and Numerical Simulation, ***NRL Memorandum Rpt., 6756-95-7734***, September 1995.

Walker, D.N., W. E. Amatucci, J. A. Antoniades, G. Ganguli, D. Duncan, J. H. Bowles, and M. E. Koepke, Perpendicular ion heating by velocity-shear-driven plasma waves, ***Geophys. Res.***

Lett., **24**, 1187 (1997).

Wang, E.Y., N. Hershkowitz, D. Diebold, T. Intrator, R. Majeski, H. Persing, G. Severn, B.Nelson, and Y. J. Yen, Secondary electron emission-capacitive probes for plasma potential measurements in plasmas with hot electrons, ***J. Appl. Phys., 61***, (10), 4786, 1987.

Whipple, E.C., Potentials of surfaces in space, ***Rep. Prog. Phys., 44***, 1197, 1981.

Winglee,R.M., Simulations of pulsed electron beam injection during active experiments, ***J. Geophys. Res., 96***, 1803, 1991.

Yau, A.W., B.A. Whalen, A.G. McNamara, P.J. Kellogg and W. Bernstein, Particle and wave observations of low altitude ionospheric ion acceleration events, ***J. Geophys. res., 88***, 3411, 1983